Churning power losses of ordinary gears: a new approach based on the internal fluid dynamics simulations

Franco Concli[1,*,†], Carlo Gorla[1], Augusto Della Torre[2] and Gianluca Montenegro[2]

[1]*Department of Mechanical Engineering, Politecnico di Milano, Via La Masa 1, I-20156 Milano, Italy*
[2]*Department of Energy, Politecnico di Milano, Via Lambruschini 4, I-20156 Milano, Italy*

INTRODUCTION

Gear power transmissions are since decades the most common way to transmit mechanical power. For this reason, thanks to years of investigations, many calculation methods are nowadays available, for example, in order to optimise the transmission again tooth braking, pitting, micropitting, wear, scuffing, etc.

Most of these failure modes are strongly related to the tribology of the system. This depends mainly on the lubricant properties that are, in turn, a function of the temperature. The new challenge in the field of gear power transmissions is to find out how to accurately calculate the operating temperature and the efficiency of the gearbox. The first step to calculate the efficiency of a gearbox is to calculate the power losses (that are dissipated in terms of heat). Literature provides many analytical and

*Correspondence to: Franco Concli, Department of Mechanical Engineering, Politecnico di Milano, Via La Masa 1, I-20156 Milano, Italy.
†E-mail: franco.concli@polimi.it

empirical relations derived from experiments in order to calculate the various contributions of the power losses. With these models, it is possible to accurately predict the losses generated, for example, by the gears due to sliding or by the bearings. What is still missing are appropriate models for the prediction of the power losses generated by the interaction between the mechanical components and the lubricant (that can represent up to 50% of the total losses[1]).

The majority of the works presented on this topic are basically just results of experimental tests. Sometimes, from the experimental results, an analytical equation is also derived. The problem of all this calculation methods is that they are accurate only as long as the real operating conditions are similar to the conditions of the experiments. Furthermore, these models often neglect some important influencing parameters.

Some work on the hydraulic losses was presented by Dowson[2] regarding the windage losses or by Mauz[3] and by Seetharaman et al.[4] who have concentrated on the churning power losses. Nevertheless, the authors maintain that a deeper understanding of the physical phenomena responsible of the losses due to the interaction with the lubricant is still needed in order to improve existing models, and CFD simulation can be an effective approach for such investigation. Marchesse et al.,[5] on the basis of a state of the art on the application of CFD to gear power losses, applied CFD models to study windage losses of gears and have validated their results by means of experimental tests. A CFD-based method was proposed also by the authors in previous papers and applied in order to study the churning losses generated by the planet carrier in a planetary gearbox.[6,7] Also, the squeezing[8,9] and the windage[9,10] power losses of ordinary gears have been deeply investigated by the authors.

This paper presents a parametric study of the churning power losses generated by a single rotating gear. Simulations were run considering different operating conditions and geometrical parameters like rotational speed, tip diameter, face width and lubricant level, in order to understand their influence on the power losses. The appropriateness of CFD as prediction tool was already validated with some experimental data in previous publications.[6,7,9,10]

COMPOSITION OF GEARBOX POWER LOSSES

According to Niemann and Winter,[11] the power losses of gears can be subdivided into load dependent and load independent losses (subscript 0).

$$P_V = P_{VG} + P_{VG0} + P_{VB} + P_{VB0} + P_{VS} + P_{VX} \tag{1}$$

This classification subdivides the losses depending on whether they are dependent from the transmitted torque or not. Another useful classification can be made according to the mechanical component that generate the losses: It can be distinguished between gear losses (subscript G), bearing losses (subscript B), seal losses (subscript S) and other generic losses like those generated by clutches or synchronizers (subscript X). A subclassification of the load independent power losses of gears P_{VG0} distinguish between windage (subscript W), churning (subscript C) and squeezing (subscript S) power losses.

The windage power losses arise due to the interaction of a mechanical component and a single phase fluid that can be either air or lubricant. These losses evolve with rotational speed power three and become significant only for high tangential speeds or for fluids with high viscosity grades and densities. The churning losses are similar to the windage ones but involve at least two phases. These losses are the

most important load independent power losses in geared transmissions: The majority of the gearboxes, in fact, are deep lubricated and, therefore, subjected to churning losses. These losses evolve with a power law less than three, but, at the actual state of the art, the knowledge regarding this contribution is very limited. The squeezing power losses are losses of a lower order of magnitude and arise due to the fact that the cavity between two teeth is reducing its volume during the engagement causing pressure gradients and, therefore, additional fluxes.

PROBLEM DESCRIPTION

In a previous paper,[10] some simple simulations have been performed with a CFD code and compared with measurements[12] showing good agreement. Once the CFD model was validated, additional simulations have been performed and the results are here presented.

The configuration of the analyzed system is quite simple. A single gear is mounted on a cantilevered shaft supported by two bearings inside a rectangular case (which dimensions can be modified) and connected to an electric motor through a shaft (and a speed increaser). The gear can be set into rotation, and the losses generated by the interaction of the gear with the air/oil lubricant mixture measured with a torque meter (speed and torque sensor) mounted between the motor and the gear as shown in Figure 1.

In this work, CFD simulations were run considering a simplified geometry of this test rig configuration. In particular, the presence of the second shaft, on which no gear is mounted, was neglected, and some other minor geometrical simplifications (e.g. chamfers) were introduced. Moreover, despite of the cantilevered shaft, the model was considered symmetric and only half of the domain has been modeled as shown in Figure 2a. These simplifications allowed us to reduce the computational burden of the simulations, without affecting the validity of the present analysis, which is aimed to the study of the effects of geometrical parameters of the gears (tip diameter and face width), oil properties and operating conditions (rotational speed and lubricant level) on the churning power losses.

For the simulation, a gear transmission mineral-based oil (FVA2) was modeled. Its properties are listed in Table I.

The adopted gears are standard C-GEARS which properties are listed in Table II.

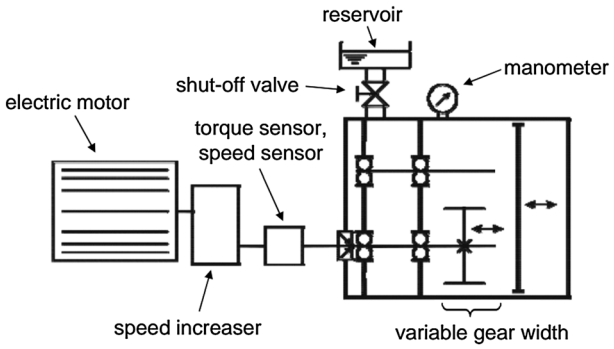

Figure 1. Schematic representation of the test rig.[10,12]

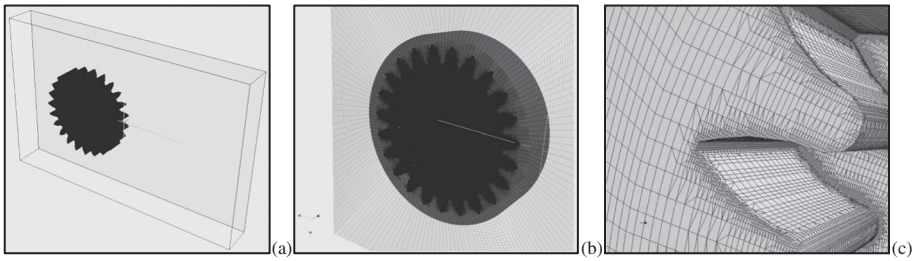

Figure 2. (a) Computational domain taking advantage of the symmetry; (b) mesh partitions; (c) detail of the mesh.

Table I. Oil properties of the used lubricants.

Oil name	Kinematic viscosity at 40 °C v_{40} [mm^2 s^{-1}]	Kinematic viscosity at 100 °C v_{100} [mm^2 s^{-1}]	Density at 15 °C ρ_{15} [kg m$^{3-1}$]
FVA2	29.8	5.2	871

NUMERICAL SIMULATIONS

For this study, an open-source code (OpenFOAM®[13]) was adopted. The choice of an open-source tool was made because it allows more flexibility with respect to close-source commercial software, making it possible to customise the code with the implementation of specific models for the analysis of the physical problem of interest.

Mesh

The main problem in performing this kind of transient simulations, at least in term of mesh handling, is to find a way to correctly describe the boundary motion corresponding to the gear rotation. In order to solve this problem, the computational domain has been split into two partitions (Figure 2b). The external one is a simple steady partition which mesh does not move during the calculations. The internal partition instead, the cylindrical one in Figure 2b, is a cell zone that rotates during the simulations. After each time step, in fact, the internal mesh is rotated of a prescribed angle, and, consequently, also the boundary motion is in this manner correctly reproduced. The advantage of this technique, called sliding mesh, is that the rotation of the gear boundaries is well reproduced avoiding mesh deformation (that means an additional computational effort).

The two partitions are numerically connected by an arbitrary mesh interface (AMI). AMI is a technique that allows simulation across disconnected, but adjacent, mesh domains. AMI operates by projecting one of the patches geometry onto the other.[13] Both domains have been discretised adopting the blockMesh and the snappyHexMesh utilities of the open-source code. In a first step, a background mesh should be created. The aspect ratio of the cells of the background mesh was approximately 1. The geometry of the gear was defined by a stereolithography (STL) file. Starting from the STL file and from the background mesh, the mesh approximately conforms to the surface by iteratively refining

Table II. Properties of the gears and lubrication of the analyzed cases.

Influencing parameters	Face width b [mm]	Tip diameter d_a [mm]	Pressure angle α_n [deg]	Number of teeth z_1	Normal module m_n [mm]	Profile shift coeff x	Lubricant level L [mm]
Reference case	40	102.5	20	23	4	−0.0615	To gear axis
Tip diameter d_a	40	96.5	20	23	4	−0.0615	To gear axis
Face width b	20	102.5	20	23	4	−0.0615	To gear axis
Lubricant level L	40	102.5	20	23	4	−0.0615	−20 (axis)—100%

the starting background mesh and morphing the resulting split-hex mesh to the surface. Once the feature and surface splitting is complete, a process of cell removal begins. The next stage of the meshing process involves moving cell vertex points onto surface geometry to remove the jagged castellated surface from the mesh. The process displace the vertices in the castellated boundary onto the STL surface, solve for relaxation of the internal mesh with the latest displaced boundary vertices, find the vertices that cause mesh quality parameters to be violated and reduce the displacement of those vertices from their initial value and repeat the operation until mesh quality is satisfied (Figure 3).

Both meshes (corresponding to the two domains) are therefore mainly made of hexaedral elements that ensure the same accuracy with a lower number of elements (that means a lot of saving in memory and computational effort) with respect to tetrahedrons. The mesh density was chosen by conducting a grid independence analysis, considering different meshes (from 10 k up to 2 M cells) in order to find the best compromise between quality of the results and computational effort. The final mesh was made of about 300 k cells.

Solver settings

In order to be able to calculate the churning power losses due to the rotation of the gear, the velocity and pressure field in the whole domain should be computed. The computational model is based on two equations that mathematically represent statements of the conservation laws of physics. The mass conservation law can be written as

$$\frac{\partial \rho}{\partial t} + \nabla \cdot (\rho \vec{v}) = 0 \tag{2}$$

where ρ is the density and $\rightarrow v$ is the velocity vector. The second equation expresses the conservation of momentum and can be written as follows:

$$\frac{\partial}{\partial t}(\rho \vec{v}) + \nabla \cdot (\rho \vec{v}\,\vec{v}) = -\nabla p + \nabla \cdot \left[\mu\left(\nabla \vec{v} + \nabla \vec{v}^{T}\right)\right] + \rho \vec{g} + \vec{F} \tag{3}$$

where p is the pressure, $\vec{v}$ is the velocity vector, ρ is the mixture density, μ is the mixture viscosity, $\vec{g}$ is the gravitational force and $\vec{F}$ represent the external forces. The adopted solver uses a PIMPLE (merged PISO-SIMPLE) algorithm. PISO is an acronym for pressure implicit splitting of operators[4] for time-dependent

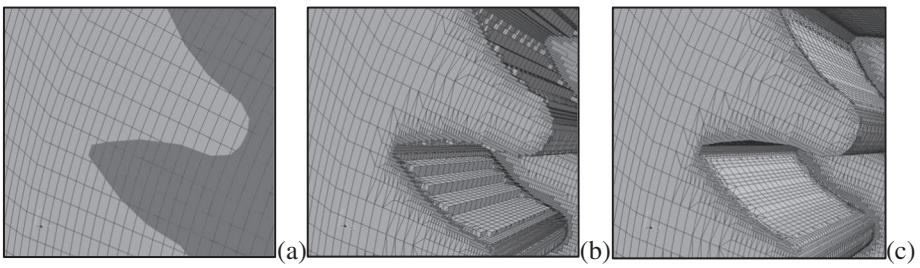

Figure 3. Steps of the meshing process: (a) geometry (STL) overlapping the background mesh; (b) castellated mesh after the cell removal process; (c) final mesh.

flows while SIMPLE stands for semi-implicit method for pressure linked equations[14] that is used for steady state problems. In the SIMPLE algorithm, a pressure correction term is used while the velocity corrections are neglected because they are unknown. This results in rather slow convergence. The PISO algorithm also neglects the velocity correction in the first step but then performs one in a later stage, which leads to additional corrections for the pressure. PIMPLE main structure is inherited from the original PISO, but it allows equation under-relaxation, as in SIMPLE, to ensure the convergence of all the equations at each time step.

The presence of more than one phase implies the need of additional equations. In particular, a transport equation for the volume fraction α is introduced:

$$\frac{\partial}{\partial t}\alpha + \frac{\partial}{\partial x_i}(\alpha u_i) = 0 \tag{4}$$

where α represents the percentage of one of the two phases (oil) in a generic cell. It assumes, therefore, the value 1 for the point x_i at the time t if the cell is completely filled with oil, 0 if the cell is completely filled with air or an intermediate value if the cell contains an air/oil mixture. Starting from the volume fraction, the mixture properties are calculated like

$$\varphi = \alpha\varphi_{oil} + (1-\alpha)\varphi_{air} \tag{5}$$

where φ represents a generic properties (ρ, μ). The mixture properties are than used in the momentum and mass conservation equations. To achieve temporal accuracy and numerical stability when running the simulations, a Courant number of 1 was adopted. The Courant number is defined as

$$Co = \frac{\delta t|\boldsymbol{U}|}{\delta x} \tag{6}$$

where δt is the time step, $|\boldsymbol{U}|$ is the magnitude of the velocity through the cell and δx is the cell size in the direction of the velocity. The time step is therefore determined considering the smaller cell size in the mesh and the maximum value in the velocity field.

These equations can be numerically solved, and the pressure and velocities in each cell center calculated. A dedicated utility (written in c++) that, starting from the velocity and pressure fields and from the mixture properties of the mixture (calculated for each cell i with the CFD code), calculates the resistant torque on the gear due to the presence of the lubricant mixture.

The basic relation on which the utility is based are

$$T_{VZ0,Ch,visc} = \sum_i \left(\nu_{mix_i}\rho_{mix_i}\frac{\delta U_i}{\delta x_i} \right) \cdot A_i \cdot r_i \tag{7}$$

$$T_{VZ0,Ch,visc} = \sum_i p_i \cdot A_i \cdot r_i \tag{8}$$

where the subscript i refers to the ith cell, ν_{mix_i} and ρ_{mix_i} are the viscosity and the density of the mixture in the cell calculated according to equation 5, A_i is the area of the cell corresponding to the boundary of the gear and r_i is the radial distance of the cell from the gear axis. $\left(\nu_{mix_i}\rho_{mix_i}\frac{\delta U_i}{\delta x_i}\right.$ represents the shear stress.

Tested conditions

Table III summarises the combination of parameters adopted for the simulations. For each geometrical configuration and static lubricant level, simulations have been performed at three different rotational speeds (2000, 5000 and 8000 rpm). Two different tip diameters (102.5 and 96.5 mm) as well as two different face width (40 and 20 mm) have been considered. In terms of lubricant quantity, three different static oil levels (0 and −20 mm with respect to the gear axis and full filling) have been taken into account.

All the simulations have been performed on a 76 GFLOPS machine and take approximately 120 h each to solve the start-up and reach the regime condition where the power losses are evaluated.

In order to speed-up the calculations, some additional simulations for a single geometrical configuration ($d_a = 96.5\ mm$, $b = 20\ mm$, $\beta = 0°$, $L = 0\ mm$) have been performed adopting a different approach: multi reference frame (MRF). The MRF model is a steady-state approximation in which individual cell zones move at different rotational speeds. The flow in each moving cell zone is solved using the moving reference frame equations in which additional terms related to the Coriolis acceleration $(2\vec{\omega}\times\vec{v_r})$ and the centripetal acceleration $(\vec{\omega}\times\vec{\omega}\times\vec{r})$ are introduced in the momentum conservation equation

$$\frac{\partial}{\partial t}(\rho\vec{v_r}) + \nabla\cdot(\rho\vec{v_r}\,\vec{v_r}) + \rho(2\vec{\omega}\times\vec{v_r} + \vec{\omega}\times\vec{\omega}\times\vec{r}) = -\nabla p + \nabla\cdot\left[\mu\left(\nabla\vec{v_r} + \nabla\vec{v_r}^{T}\right)\right] + \rho\vec{g} + \vec{F} \qquad (9)$$

where p is the pressure, ρ is the mixture density, μ is the mixture viscosity, $\vec{g}$ is the gravitational force, $\vec{F}$ represents the external forces, $\vec{\omega}$ is the angular velocity relative to a stationary (inertial) reference frame and $\vec{v_r}$ is defined as $\vec{v_r} = \vec{v} - \vec{\omega}\times\vec{r}$ where $\vec{r}$ is the position vector from the origin of the rotating frame. Also, the continuity equation is modified and written in terms of relative velocities

$$\frac{\partial\rho}{\partial t} + \nabla\cdot(\rho\vec{v_r}) = 0 \qquad (10)$$

At the interfaces between cell zones, a local reference frame transformation is performed to enable flow variables in one zone to be used to calculate fluxes at the boundary of the adjacent zone. It should be noted that the MRF approach does not account for the relative motion of a moving zone with respect to adjacent zones; the grid remains fixed for the computation. This is analogous to freezing the motion of the moving part in a specific position and observing the instantaneous flow field with the rotor in that position. While the MRF approach is clearly an approximation, it can provide a reasonable model of the flow for many applications and allows a drastically reduction of the computational effort with respect to the sliding mesh approach. However, the multiple reference frame model does not accurately simulate the transient start-up but gives just a regime solution of an unsteady problem. This approach cannot, therefore, be applied for the study of the phenomena occurring during the start-up but represents a good alternative if the target is just to calculate the power losses at the regime and can be very useful in the industrial practice where computational time is an important issue. Furthermore, for this specific application, the results obtained with this approximated method are in agreement with the results obtained simulating the whole start-up.

RESULTS

Figure 4 shows the results of the simulations in terms of churning torque versus rotational speed. Figure 4a shows the influence of the tip diameter on the losses. This parameter seems to be the most

Table III. Combination of parameters adopted in the different simulations.

Sliding mesh—AMI approach							
Influencing parameter	Tip diameter d_a [mm]	Face width b [mm]	Rotational speed n [rpm]	Normal module m_n [mm]	Temperature θ [°C]	Oil level* L[mm]	Oil type
Reference case	102.5	40	2000	4	90	0	FVA2
	102.5	40	5000	4	90	0	FVA2
	102.5	40	8000	4	90	0	FVA2
Tip diameter d_a	96.5	40	2000	4	90	0	FVA2
	96.5	40	5000	4	90	0	FVA2
	96.5	40	8000	4	90	0	FVA2
Face width b	102.5	20	2000	4	90	0	FVA2
	102.5	20	5000	4	90	0	FVA2
	102.5	20	8000	4	90	0	FVA2
Lubricant level L	102.5	40	2000	4	90	−20	FVA2
	102.5	40	5000	4	90	−20	FVA2
	102.5	40	8000	4	90	−20	FVA2
	102.5	40	2000	4	90	Full (100)	FVA2
	102.5	40	5000	4	90	Full (100)	FVA2
	102.5	40	8000	4	90	Full (100)	FVA2
MRF approach							
Influencing parameter	Tip diameter d_a [mm]	Face width b [mm]	Rotational speed n [rpm]	Normal module m_n [mm]	Temperature θ [°C]	Oil level* L[mm]	Oil type
Tip diameter d_a	96.5	40	2000	4	90	0	FVA2
	96.5	40	5000	4	90	0	FVA2
	96.5	40	8000	4	90	0	FVA2

*the oil level is calculated from the gear axis

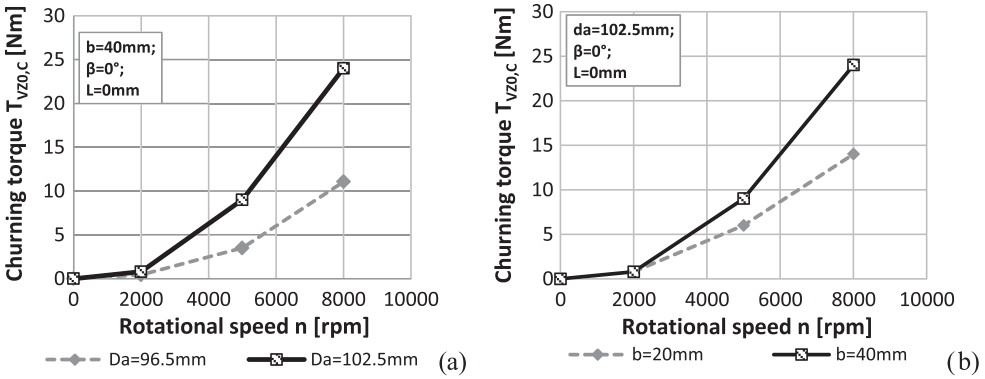

Figure 4. Effect of the geometrical parameters on the churning power losses: (a) tip diameter influence; (b) face width influence.

influencing one on the churning power losses: An increment of the tip diameter from 96.5 to 102.5 mm (about 5%), in fact, induces an increment of about 100% in the churning torque.

Figure 4b shows the influence of the face width on the churning losses. As expected, a halving of the face width does not mean a halving of the losses due to the side effects that remain the same. The influence of these two geometrical parameters is very similar to the trends shown for a single phase lubrication.[7] The main difference is the influence of the rotational speed on the losses: Unlike the windage losses, the churning ones evolve with rotational speed power less than three.

Figure 5 shows the influence of the static lubricant level on the churning losses. The dots represent the condition of completely filled gearbox (oil-windage losses). This condition is very uncommon but sometimes needed, for example, in the case of applications operating at the bottom of the sea where the external pressure should be compensated in order to prevent a structural collapse. A reduction of the lubricant level implies a strong reduction of the losses. In this case, the halving of its quantity induces

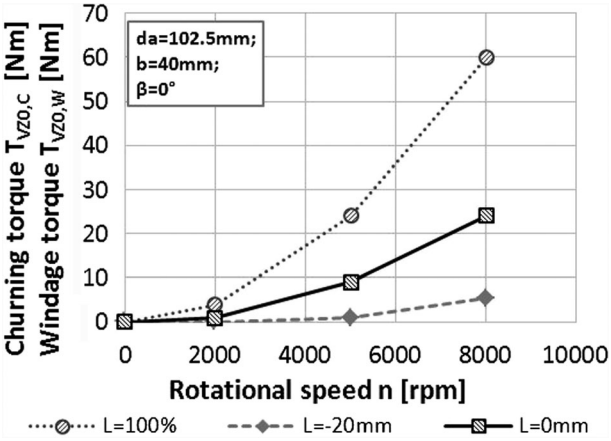

Figure 5. Effect of the static lubricant level on the churning power losses.

a reduction of about 60% of in the losses (continuous line). An additional reduction of 20 mm (approximately 25% filling) of the static oil level (broken line) implies a further reduction of the losses of about 70% with respect to the case with 50% oil filling. In this last case, in the steady condition, only few teeth are immersed in the lubricant, and therefore, a smaller fraction of oil is involved in the phenomena.

These results points out the importance to correctly choose the right amount of lubricant in order to minimise the power losses but, at the same time, to avoid thermal and lubrication problems. However, the magnitude of the reduction is strongly dependent from the gearbox configuration: In this case, the gearbox internal volume was limited and the oil was forced to remain in proximity of the gear (Figure 6) and, therefore, to interact with it. In design solutions with more space inside the gearbox (Figure 7), a reduction of the amount of oil implies also much bigger reductions of the losses.

Figure 7 clearly shows this fact: An increment of the shrouding box sizes from 35x290xh185 (Figure 6) to 100x600xh400 mm (Figure 7) maintaining the gear sizes implies a reduction of the losses of about 68%. Figure 7b shows also clearly that the lubricant circulation is completely different from the case with a smaller internal volume (Figure 6d). This kind of comparison indicates clearly another advantage offered by CFD simulations: The ability to study systems where controlled experiments are difficult or impossible to perform. In the industrial practice, in fact, often happens that some prototypes result to not being well lubricated.

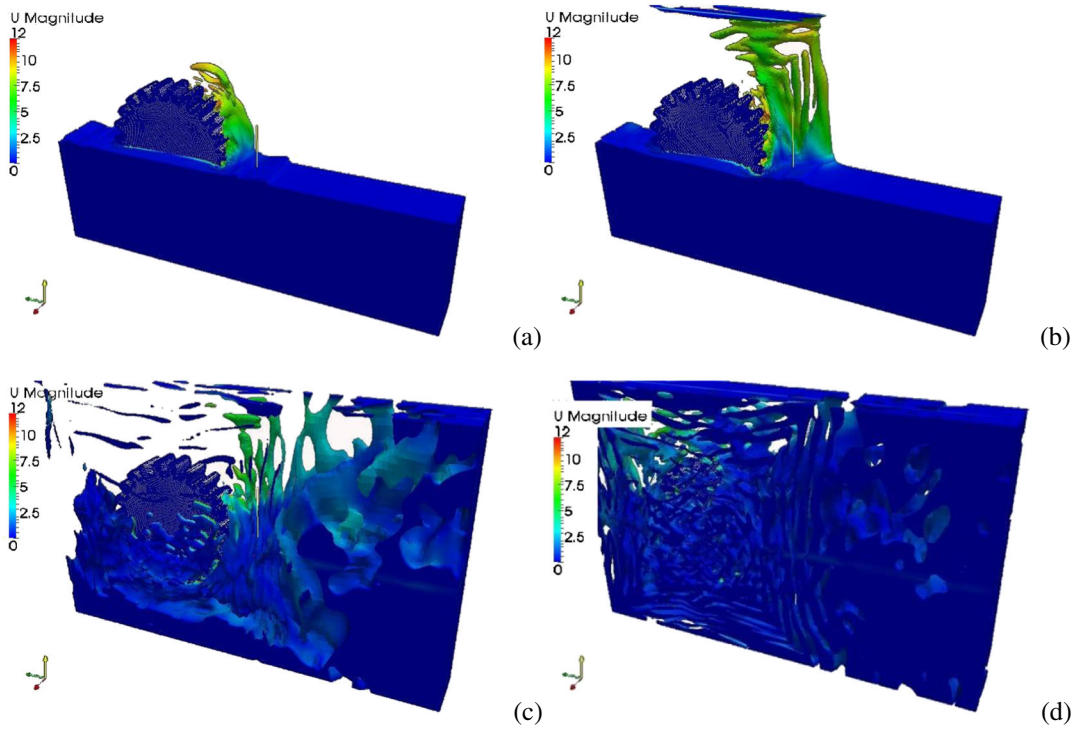

Figure 6. (a), (b), and (c) Start-up: Velocity contour plot of the lubricant phase at different time steps; (d) regime condition.

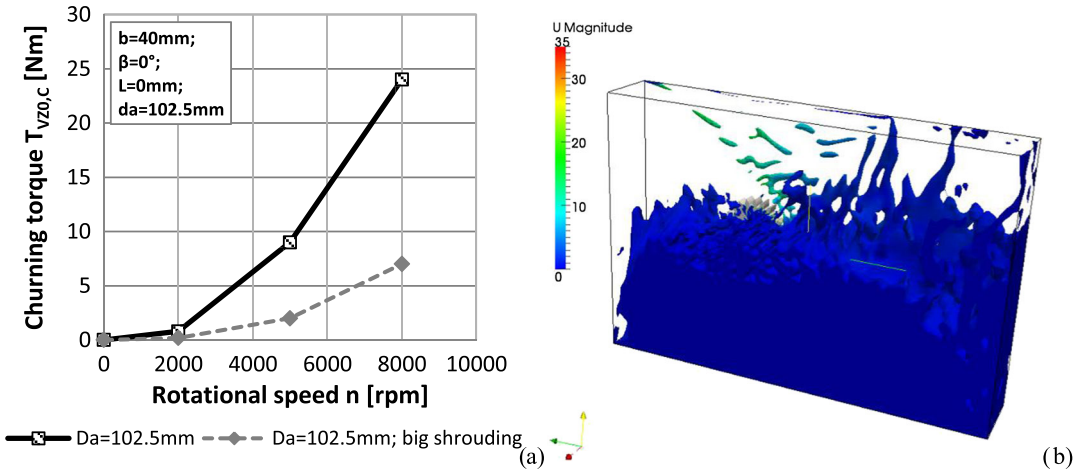

Figure 7. (a) Effect of the internal volume on the power losses; (b) velocity contour plot of the lubricant phase with a bigger internal volume (regime).

On a test rig is quite difficult to study the fluxes of lubricant inside the case and to prove the effectiveness of each modification since a new prototype should be realised and tested. Conversely, CFD allows engineers to deeply understand the internal fluid dynamics of the gearbox, making easier the choice of the best solution for a lubrication problem and allowing an immediate virtual test of any new configuration. Figure 8a and 8b shows the oil distribution and the pressure distribution on the surfaces of the gear in the case with a partial lubricant filling. A comparison of the pressure distribution in a dip lubrication condition with the pressure for the same operating conditions but with one single phase (8c) shows how the two phenomena (churning and windage) are completely different. In the windage (8c), the pressure depends only from the rotational direction and speed (points s1, s1 and s3) while when churning arise (8a/b), the pressure distribution is strongly dependent also from the lubricant distribution. Peaks of pressure, in fact, arise where the volume fraction of the lubricant is higher due to its inertial effects (Figure 8a and 8b points m1 and m2).

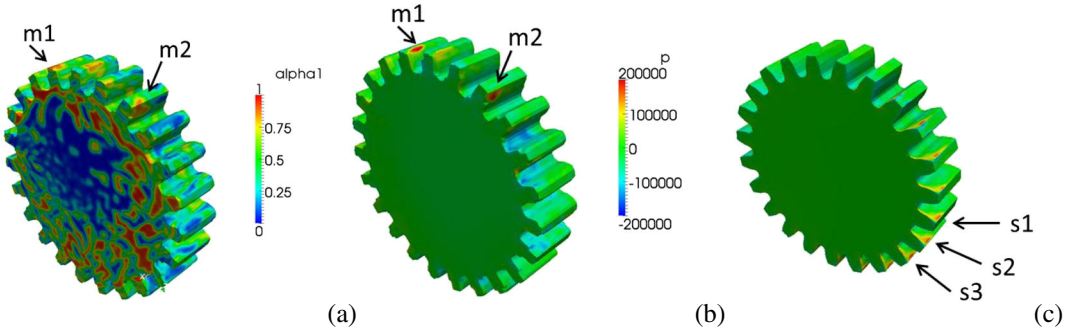

Figure 8. (a) Volume fraction contour plot; (b) pressure contour plot (two phases); (c) pressure contour plot (one phase).

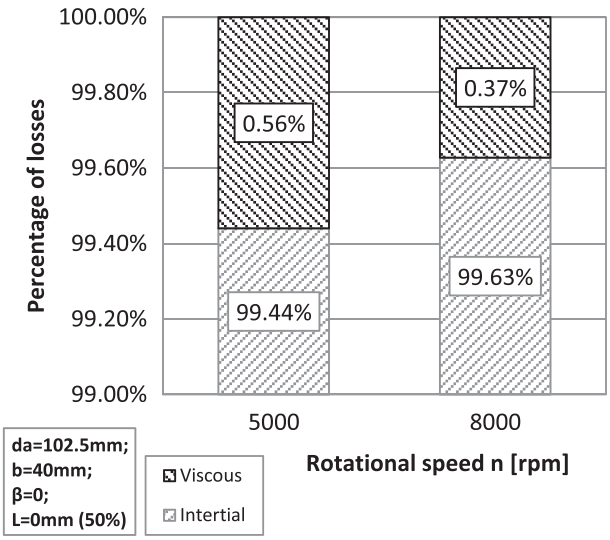

Figure 9. Decomposition of the losses for two different rotational speeds.

This fact points out, once again, the importance to be able to describe the dynamic of the fluids for the prediction of the power losses. The losses, in fact, arise both due to pressure and shear contributions, but the pressure effects are of a higher order of magnitude as shown in Figure 9.

Due to the complexity of the phenomena, it is very complicated to extrapolate analytical or empirical models that are able to well predict the losses (and therefore indirectly the fluid behavior), especially when more than one phase are involved. For this reason, the authors maintain that this kind of approach based on CFD can be an effective approach for this kind of investigation. It is in fact applicable to each specific design and operating conditions giving more accurate results than any available empirical model. Furthermore, in comparison with experiments, this approach is cheaper and less time-consuming and provides more information on the physical phenomena than any measurement. For this reason, it can give big improvements to the power loss reduction especially if adopted already during the design stage of complex gearboxes.

CONCLUSIONS

A CFD open-source code has been adopted in order to study the influence of some operating and geometrical parameters on the churning power losses of gears. The adopted model was previously validated[10] with experimental tests.

From the results of the simulations, it can be seen that the tip diameter as well as the face will have an enormous influence on the power losses. The lubricant level has also a big influence; in this specific geometrical configuration, a halving of the amount of lubricant implies a reduction of about 60% of the losses, but if the volumes inside the gearbox increase, the reduction can be also more significant. These considerations point out the importance to be able to optimise the gearbox using predictive models. Reducing the power losses, in fact, means reducing the operating temperatures and, therefore, improving the system reliability.

Due to the complex internal fluid dynamics, the empirical models provided by literature often give results that cannot be trusted. Nevertheless, being able to predict the power losses avoiding or reducing the need of prototyping and testing can give big advantages in terms of costs and developing times to gearbox manufacturers. For this reason, the authors maintain that the here proposed approach, with the two possible ways of calculations (AMI and MRF) can be effectively used as advanced design tool in the field of gear transmissions.

The aims of this study are both to provide data that can be effectively used by engineers in the design practice for a first rough estimationand also to prove, once again, CFD to be an effective approach for this kind of investigations that provide to engineers a lot of useful and detailed data regarding the power loss mechanism.

These results will be the basis for a larger research program regarding all the no-load power losses of gears in which also the real condition concerning more than one single rotating gear (mating gear pair) will be studied and simulated.

REFERENCES

1. Strasser D. Einfluss des Zahnflanken und Zahnkopfspieles auf die Leerlaufverlustleistung von Zahnradgetrieben Bochum, 2005.
2. Dawson PH. Windage loss in larger high-speed gears. *Proceedings of the Institution of Mechanical Engineers* 1984; **198**(1):51–59.
3. Mauz W. Hydraulische Verluste von Stirnradgetrieben bei Umfangsgeschwindigkeiten bis 60 m/s, Universität Stuttgart 1987.
4. Seetharaman S, Kahraman A, Moorhead MD, Petry-Johnson TT. Oil Churning Power Losses of a Gear Pair: Experiments and Model Validation. *Journal of Tribology* 2009; **131**(2):022202-1–022202-10.
5. Marchesse Y, Changenet C, Ville F, Velex P. Investigation on CFD simulation for predicting windage power losses in spur gears. *ASME Journal of Mechanical Design* 2011; **133**(2):7.
6. Concli F, Gorla C. Computational and experimental analysis of the churning power losses in an industrial planetary speed reducers. In: Proceedings of the 9th international conference on advances in fluid mechanics – advances in fluid mechanics IX. *WIT Transactions on Engineering Sciences* 2012; **74**:287–298. ISSN: 17433533; ISBN: 978-184564600-4
7. Concli F, Gorla C. Influence Of Lubricant Temperature, Lubricant Level And Rotational Speed On The Churning Power Loss In An Industrial Planetary Speed Reducer: Computational And Experimental Study. *International Journal of Computational Methods & Experimental Measurements* **1**(4). ISSN: 2046-0554
8. Concli F, Gorla C. Oil squeezing power losses of a gear pair: a CFD analysis. In: Proceedings of the 9th international conference on advances in fluid mechanics – advances in fluid mechanics IX. *WIT Transactions on Engineering Sciences* 2012; **74**:37–48. ISSN: 17433533; ISBN: 978-184564600-4
9. Gorla C, Concli F, Stahl K, Höhn B-R, Michaelis K, Schultheiß H, Stemplinger J-P. Hydraulic losses of a gearbox: CFD analysis and experiments. *Tribology International* 2013; **66**:337–344.
10. Gorla C, Concli F, Stahl K, Höhn B-R, Michaelis K, Schultheiß H, Stemplinger J-P. CFD simulations of splash losses of a gearbox. Tribological challenges in mechanical transmissions. Special issue of "Advances in Tribology". Article number 616923, HINDAWI 2012. ISSN: 1687–5915
11. Niemann G, Winter H. Maschinenelemente Band II – Getriebe allgemein, Zahnradgetriebe – Grundlagen, Stirnradgetriebe, Springer-Verlag, Berlin Heidelberg Ney York Tokio 1983. ISBN: 3540111492
12. Hohn BR, Michaelis K, Otto HP. Influence on no-load gear losses, in Proceedings of the *Ecotrib Conference*, Volume **2**, 2011: 639–644.
13. The open source CFD toolbox, official documentation. http://www.openfoam.com
14. Versteeg HK, Malalasekera W. An introduction to computational fluid dynamics – the finite volume method, Longman Group, London 1995. ISBN: 9780131274983